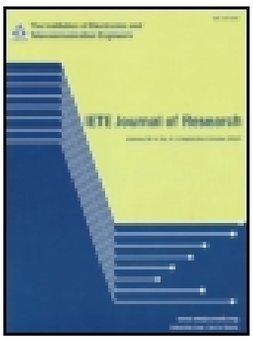

IETE Journal of Research

ISSN: 0377-2063 (Print) 0974-780X (Online) Journal homepage: http://www.tandfonline.com/loi/tijr20

QRS Complex Detection in ECG Signals Using the Synchrosqueezed Wavelet Transform

Tanushree Sharma & Kamalesh K. Sharma

To cite this article: Tanushree Sharma & Kamalesh K. Sharma (2016): QRS Complex Detection in ECG Signals Using the Synchrosqueezed Wavelet Transform, IETE Journal of Research, DOI: 10.1080/03772063.2016.1221744

To link to this article: http://dx.doi.org/10.1080/03772063.2016.1221744

Published online: 07 Sep 2016.

IETE JOURNAL OF RESEARCH, 2016
http://dx.doi.org/10.1080/03772063.2016.1221744

QRS Complex Detection in ECG Signals Using the Synchrosqueezed Wavelet Transform

Tanushree Sharma and Kamalesh K. Sharma

Department of Electronics and Communication Engineering, Malaviya National Institute of Technology, Jaipur, India

ABSTRACT

The QRS complex is the most distinctive feature in an electrocardiogram (ECG) signal. Therefore, its detection serves as the starting point for various applications, such as detection of other waves and segments, heart-rate calculation, derivation of respiration, etc. In this paper, a novel technique for QRS detection is proposed. The technique is based on the recently proposed synchrosqueezed wavelet transform (SSWT), which is obtained by application of a post-processing technique known as *synchrosqueezing* to the continuous wavelet transform. Following SSWT, various other processing steps are applied, including a nonlinear mapping technique, which is novel in the context of QRS detection, to finally detect the R-peaks. The proposed algorithm is evaluated on the MIT-BIH arrhythmia database and overall sensitivity, positive predictivity and error rate obtained are 99.92%, 99.93%, and 0.15%, respectively.

KEYWORDS

Biomedical signal processing; ECG; QRS; Time frequency representation; Signal processing; Wavelet transform

1. INTRODUCTION

The electrocardiogram (ECG) is an electrical manifestation of the contractile activity of the myocardium or heart muscle, which is measured from the body surface of the subject using electrodes [1]. It is a very commonly used non-invasive test for diagnosis of cardiovascular abnormalities. The QRS complex is the most distinguishable pattern in the ECG signal, and therefore, its detection usually serves as the reference for locating other waves and segments [2,3]. It is often used for beat segments extraction for the purpose of classification [4–6]. Also, it is required for calculating the R–R interval, which is used in heart-rate variability analysis [7,8]. QRS detection is not a simple peak-finding problem. Difficulties arise in QRS detection due to factors such as muscular noise, electrode artefacts, baseline drift, pathological signals, low signal-to-noise ratios, QRS-like artefacts, and tall P- and T-waves [9]. A detailed review on the numerous approaches for QRS detection proposed in the literature is given in [9]. The algorithmic structure generally used in most automated QRS detection algorithms consists of a pre-processing or feature extraction stage including linear and nonlinear filtering and a decision stage, which includes peak detection and a decision logic [9]. The decision stages are usually heuristic and dependent on the results of the pre-processing stage. Various pre-processing techniques have been proposed in the literature, such as the derivative-based technique used in the classic and popular algorithm proposed by Pan and Tompkins in [10]. Numerous other pre-processing techniques have also been proposed, including those based on artificial neural networks [11–13], wavelet transforms [14–17], quadratic filter [18], S-transform [19], sparse derivatives [20] and Shannon energy envelope [21,22].

In this paper, a QRS detection technique based on the synchrosqueezed wavelet transform (SSWT) is proposed. SSWT is obtained from the continuous wavelet transform (CWT) by application of a frequency-reassignment technique known as *synchrosqueezing*, resulting in higher resolution. While the CWT gives a time-scale representation of a signal, the SSWT gives its time-frequency representation (TFR). The SSWT has been shown to be largely invariant to the choice of the mother wavelet [23], unlike the CWT. Also, thresholding of the wavelet coefficients is part of the SSWT implementation process, which aids in removal of additive Gaussian noise. The SSWT has recently been used for various applications such as the analysis of seismic signals [24,25], paleoclimate records and incoming solar radiation (insolation) [23] and damping identification in a vibration system [26]. In the context of ECG signals, it has been used for obtaining breathing dynamics from ECG signals [27] and for diagnosis of paroxysmal atrioventricular block using the ECG [28]. Its application to QRS detection in ECG signals, however, has not yet been explored. An overview of the SSWT is provided in Section 2. Section 3 describes the methodology and in Section 4 the experimental results are presented. Finally, Section 5 concludes the paper.

2. REVIEW OF THE SYNCHROSQUEEZED WAVELET TRANSFORM

Synchrosqueezing was originally introduced in the context of analysing auditory signals [29]. It is a special case of reallocation methods [30–32], which aim to "sharpen" a TFR, i.e. enhance its resolution. Synchrosqueezing was recently further studied in [33] and shown to capture the flavour and philosophy of the empirical mode decomposition (EMD) [34], albeit using a different approach, and a firm theoretical foundation, which is not available for EMD. Also, it allows exact reconstruction of constituent components, like EMD and unlike classical TFR techniques [23]. A brief overview of wavelet-based synchrosqueezing, originally described in [33], is given below. A more detailed description can be found in [33].

To obtain the SSWT, one starts with the CWT of a signal $s(t)$, given by

$$W(a,b) = \int a^{-1/2}\psi^*\left(\frac{t-b}{a}\right)s(t)dt, \tag{1}$$

where $W(a,b)$ are wavelet coefficients, a is the scale parameter, b is the translation parameter, and $\psi^*(t)$ denotes the complex conjugate of the mother wavelet $\psi(t)$.

For every (a,b) under consideration, for which $W(a,b) > \gamma$, instantaneous frequency,

$$\omega_s(a,b) = -i(W(a,b))^{-1}\frac{\partial}{\partial b}W(a,b) \tag{2}$$

is computed, where γ is a threshold chosen as described in the next section. $\omega_s(a,b)$ can be considered to be an "FM demodulated" estimate that cancels out the effect of the mother wavelet on the wavelet coefficients [23]. In the next step, the information from the time-scale plane is mapped to the time-frequency plane, according to the map $(b,a) \to (b, \omega_s(a,b))$ in an operation termed "synchrosqueezing." The SSWT, $T_s(\omega,b)$, is given by [33]

$$T_s(\omega,b) = \int_{A(b)} W(a,b)a^{-3/2}\delta(\omega_s(a,b)-\omega)da, \tag{3}$$

where $A(b) = \{a;\ W(a,b) \neq 0\}$ and $\delta(\cdot)$ is the Dirac delta function. The signal $s(t)$ can be recovered from its SSWT using the reconstruction formula:

$$s(t) = \mathcal{R}e\left[C'_\Psi \int_0^\infty T_s(\omega,t)\ \mathrm{d}\omega\right], \tag{4}$$

where C'_Ψ is a constant that depends only on Ψ [33].

3. METHOD

A schematic representation of the proposed method is shown in Figure 1. The various processing steps used are described below.

Step-1: In the first step, the SSWT of the signal is obtained. The digitized ECG signal $\tilde{s}(m)$, $m = 0, \ldots, M-1$, is a uniform discretization of the continuous time ECG signal $s(t)$ sampled at the time instants $t_m = t_0 + m\Delta t$. To prevent boundary effects, $\tilde{s}(m)$ is symmetrically padded on both sides, by using reflecting boundary conditions and converted in the form of a vector $\tilde{s}_p \in R^n$, $n = 2^{L+1}$, where L is a non-negative integer [23]. The maximum measurable frequency (Nyquist frequency) of the signal $\tilde{s}_n$ is given by $f_M = 1/2\Delta t$, where Δt is the sampling interval and the minimum measurable frequency (fundamental frequency) is given by $f_m = 1/T$, where $T = (M-1)\Delta t$ is the signal duration. The SSWT of the signal $\tilde{s}_p$ is obtained over linearly spaced frequencies ranging from f_m to f_M. The total number of frequencies considered is $n_f = Ln_v$, where n_v is a user defined parameter, known as the voice number [23].

A hard-threshold parameter $\gamma > 0$ is chosen which effectively decides the lowest CWT magnitude at which the

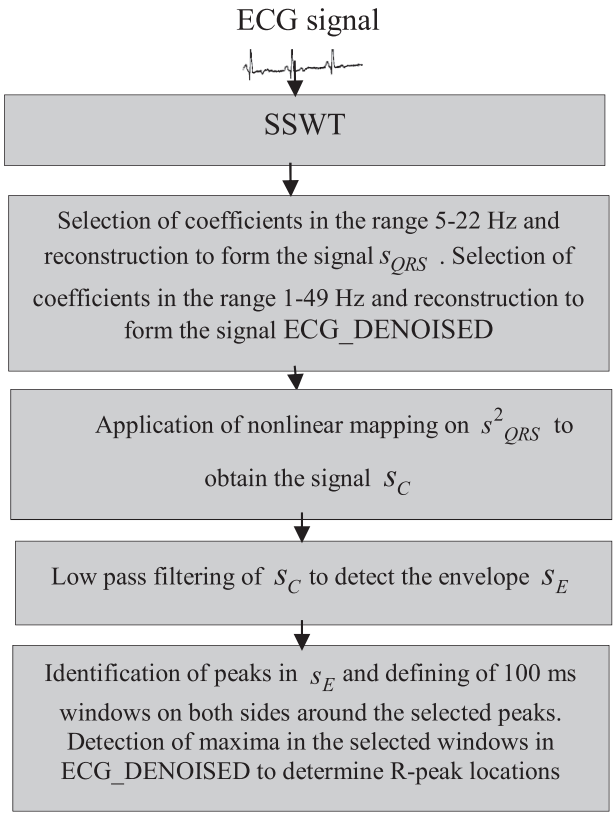

Figure 1: Schematic representation of the overall technique

instantaneous frequency can be reliably computed. Any points where $|W(a,b)| \leq \gamma$ are disregarded in SSWT computation [23]. Thus, γ can be seen as a hard threshold on the wavelet representation, whose value determines the level of filtering. In [23], Thakur et al. have suggested the use of the threshold:

$$\gamma = 1.4826\sqrt{2\log n}\cdot\mathrm{MAD}\ (|\tilde{W}_{\tilde{f}}|_{1:n_v}), \tag{5}$$

where MAD denotes median absolute deviation of $|\tilde{W}_{\tilde{f}}|_{1:n_v}$ which are the wavelet coefficients at the n_v finest scales and 1.4826 is a multiplicative constant that relates the Gaussian distribution to its standard deviation. In this work, we have used only the aforementioned thresholding operation in SSWT computation, which aids in filtering Gaussian noise. However, it is worth mentioning that some techniques have been proposed in the literature that can be used to obtain a better TFR with a sharp localization of components and reduced noise fluctuations. For example, in [35], multitapering is applied to reassigned spectrograms, which leads to coherent averaging of the chirp components and incoherent averaging in the noise regions, thereby leading to smoothing of the noise fluctuations. In [36], synchrosqueezing a highly redundant time-frequency transform with over-complete samples in a and different mother wave packets have been suggested. This generates many estimates from a single realization of noisy signal. Since the estimation of the instantaneous frequency is independent of a and the mother wavelet/wave packet, therefore, these estimates can be averaged to give a better result because of coherent averaging for signal components and incoherent averaging for noise. The use of different mother wave packets is essentially the same as multitapering [36].

An ECG signal and its TFR obtained using the SSWT are shown in Figure 2, for illustration. It can be seen that the individual QRS complexes are well localized in time in the SSWT.

Step-2: The energy of the QRS complex is found to be concentrated in the frequency range 5–22 Hz [16]. Hence, SSWT coefficients corresponding to this frequency range are reconstructed by taking inverse SSWT, to obtain the signal s_{QRS}. It is worth mentioning that recently, some reconstruction issues with SSWT have been highlighted [37], when component retrieval from ridge in the TFR is required. In fact, the recently proposed synchrosqueezed wave packet transform [38] has been shown to have a higher resolution and much superior component identification ability as compared to the SSWT. However, in the present case, the specific

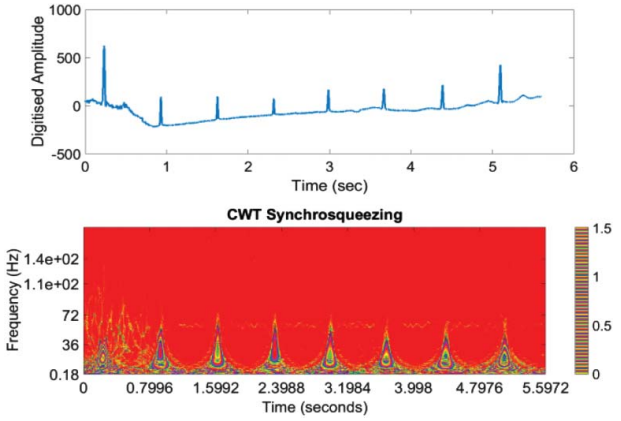

Figure 2: ECG signal and the corresponding SSWT (top) ECG signal (bottom) corresponding SSWT

frequency range is directly reconstructed, as the individual QRS complexes are well localized in time in this range, i.e. no ridge retrieval is used. Hence, no reconstruction issue arises in the present case. It may be noted that the selection of this frequency band automatically excludes baseline wander, which lies at frequencies below 1 Hz and the high frequency noise. Also, low frequency P- and T-waves, which could have amplitudes larger than the QRS complex, are suppressed. Another signal, ECG_DENOISED is also obtained, by reconstruction using coefficients in the frequency range 1–49 Hz. Figure 3 shows an ECG signal and the signal s_{QRS} obtained from it. The signal ECG_DENOISED is also shown in the bottom.

Step-3: As a result of the filtering operation in the previous step using the SSWT, the P- and T-waves and the noise peaks are greatly suppressed. However, there are still very low amplitude contributions from these peaks which need to be further suppressed in order to avoid false detections. For this purpose, the signal s_{QRS} is further processed in a series of steps. First, the signal s_{QRS} is squared and then a nonlinear mapping is applied to s^2_{QRS}, as follows:

$$s_C = s_{\max}\frac{\ln[1+\mu(s^2_{\mathrm{QRS}}/s_{\max})]}{\ln(1+\mu)}, \tag{6}$$

where $s_{\max}$ is the maximum value of s^2_{QRS} and μ is a positive constant. It may be noted that Equation (6) may be seen as the well-known μ-law logarithmic compression used in pulse code modulation systems, applied to the square of the signal s_{QRS}. To the best of our knowledge, it has not been used in the context of QRS detection earlier. The squaring operation makes all data points positive, further suppresses the undesired low amplitude peaks, and boosts the higher amplitude QRS complex peaks, as is evident from Figure 3(c). However, as an undesirable effect, this also further attenuates the low amplitude QRS

complexes. Therefore, to compensate for squaring operation, logarithmic compression is applied, which basically boosts the low and medium intensity QRS complexes, to bring their amplitudes closer to the highest amplitude complexes. Thus, the range of variations of the input is compressed. This is illustrated in Figure 3(d), where it can be seen that the QRS amplitudes have been equalized. How logarithmic compression achieves this equalization can be understood with the help of the curves in Figure 4, in which the logarithmically compressed output $s_C$is plotted against the normalized input $s^2{}_{\mathrm{QRS}}/s_{\max}$ for various values of compression factor μ. For reference, the case of no compression ($\mu = 0$) is also shown. It is seen that as μ is increased, the low and mid-range

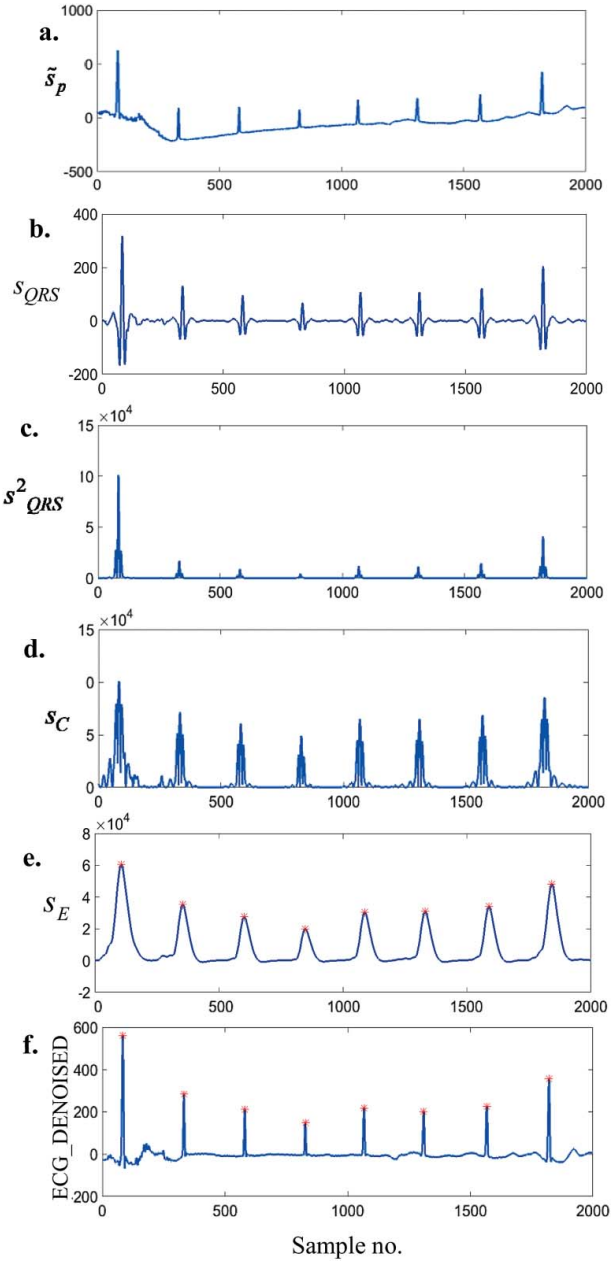

Figure 3: Signals obtained at various stages of processing for R-peak detection

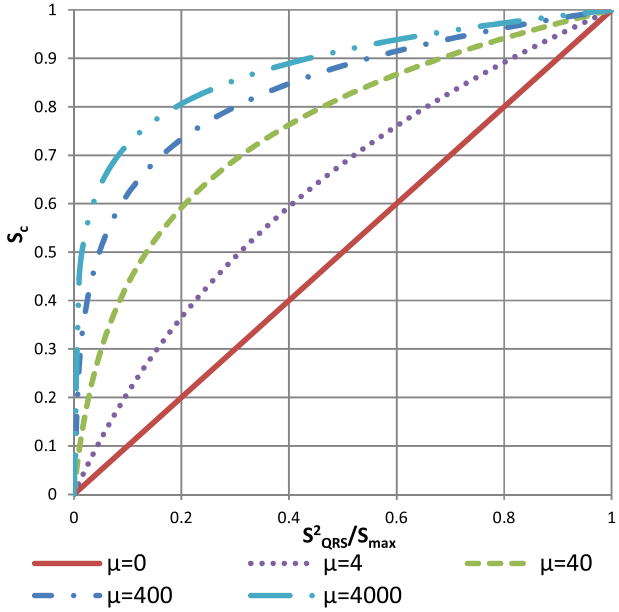

Figure 4: Logarithmic compression curves for different values of μ.

intensities are boosted more and more. In this work, $\mu = 400$ is empirically found to be an appropriate value. The reason why this equalization is required is as follows. The threshold used in this work for QRS detection is fixed and dependent on the maximum (peak) value of the signal under consideration. As such, if a very large amplitude QRS complex occurs along with a very small QRS complex in the signal duration under consideration, false negatives may occur as a result of failed detection of the small QRS complexes. Logarithmic compression boosts the low and mid-range amplitude QRS complexes, thereby reducing the false negatives.

Step-4: After application of nonlinear mapping, the envelope s_E of the signal s_C is extracted using a low pass filter, as shown in Figure 3. In this work, a second order Butterworth filter with cut-off frequency 3.6 Hz has been used.

Step-5: In the final step, the peaks are detected in the envelope signal. For the purpose of peak detection, three detection parameters: threshold, minimum peak separation and minimum peak prominence are used. The threshold is empirically determined and set to 27% of the maximum value of the envelope signal. The minimum peak separation is set as 200 ms. This is chosen because of the physiologically determined refractory period of 200 ms between two consecutive QRS complexes [10]. Another parameter, *peak prominence* is also used that measures how much the peak stands out due to its intrinsic height and its location relative to other peaks. The minimum peak prominence is set to 33% of

the peak value of the envelope signal. The use of this parameter is found to significantly reduce the number of false positives. Finally, in each beat, windows of 100 ms are defined around the detected peaks on both sides. The maxima occurring in these windows in the signal ECG_-DENOISED are determined as R-peaks, as shown in Figure 3. It may be noted that the peaks are detected in the signal ECG_DENOISED instead of the initial ECG signal, because the initial ECG can contain baseline wander, which could lead to erroneous detection of peaks. The example ECG used in Figure 3 does not have high baseline wander, muscular noise or other artefacts. The performance of the proposed method when these interferences are present is shown in the next section.

4. RESULTS AND DISCUSSION

The proposed technique is evaluated on the MIT-BIH arrhythmia database [39]. In this database, 48 annotated recordings of 30 minutes duration from two channels are available for every record. The recordings are digitized at 360 samples per second. The first channel corresponding to the modified limb lead II is used in this work. For SSWT computation, the MATLAB Synchrosqueezing Toolbox [40] by Thakur et al. [23] has been used. The SSWT has been computed using the bump wavelet over dyadic frequencies, with 64 log-spaced bins per octave, i.e. $n_v = 64$.The algorithm is applied on the ECG signal taking three-second segment at a time, so that an outlier high amplitude peak in any segment does not affect threshold value for the entire signal. In this sense, the threshold can be considered to be locally adaptive. To evaluate the efficacy of the proposed technique, three parameters: sensitivity (Se), positive predictivity (P^+), and error rate (Er) are used, which are defined as follows:

$$\mathrm{Se} = \frac{\mathrm{TP}}{\mathrm{TP} + \mathrm{FN}} \times 100\% \tag{7}$$

$$P^+ = \frac{\mathrm{TP}}{\mathrm{TP} + \mathrm{FP}} \times 100\% \tag{8}$$

$$\mathrm{Er} = \frac{\mathrm{FP} + \mathrm{FN}}{\mathrm{TB}} \times 100\%, \tag{9}$$

where TP denotes the number of true positives, i.e. correctly detected R-peaks, FN denotes the number of false negatives, i.e. failure to detect an R-peak, FP denotes the number of false positives, i.e. a falsely detected R-peak and TB denotes the actual total number of beats. The experimental results are shown in Table 1. Overall sensitivity, specificity and error rate values of 99.92%, 99.93%, and 0.15%, respectively, are obtained. To demonstrate the QRS detection ability of the proposed algorithm on ECG signals containing different wave morphologies and different kinds of noise, its performance on some selected ECG segments from different records is illustrated. Figure 5 shows the performance of the algorithm on a segment from record 104 containing muscular noise. The detected peaks are marked with asterisk. As can be seen, all peaks are successfully detected with no false positives due to noise peaks. Figure 6 shows another ECG segment containing large baseline wander. Again, the R-peaks are successfully detected. The frequency content of QRS complexes can vary because of different morphologies. Figure 7 shows the performance of the

Table 1: Experimental results of QRS detection on MIT-BIH database

Record	Total beats	TP	FP	FN	Se (%)	P^+ (%)	Er (%)
100	2273	2273	0	0	100.00	100.00	0.00
101	1865	1863	3	2	99.89	99.84	0.27
102	2187	2187	0	0	100.00	100.00	0.00
103	2084	2084	0	0	100.00	100.00	0.00
104	2229	2228	5	1	99.96	99.78	0.27
105	2572	2567	5	10	99.61	99.81	0.58
106	2027	2026	2	1	99.95	99.90	0.15
107	2137	2137	0	0	100.00	100.00	0.00
108	1763	1742	13	21	98.81	99.26	1.93
109	2532	2532	0	0	100.00	100.00	0.00
111	2124	2124	0	0	100.00	100.00	0.00
112	2539	2539	0	0	100.00	100.00	0.00
113	1795	1795	0	0	100.00	100.00	0.00
114	1879	1878	1	1	99.95	99.95	0.11
115	1953	1953	1	1	99.95	99.95	0.10
116	2412	2401	7	13	99.46	99.71	0.83
117	1535	1535	0	0	100.00	100.00	0.00
118	2278	2278	0	0	100.00	100.00	0.00
119	1987	1987	0	0	100.00	100.00	0.00
121	1863	1862	0	1	99.95	100.00	0.05
122	2476	2476	0	0	100.00	100.00	0.00
123	1518	1518	0	0	100.00	100.00	0.00
124	1619	1619	0	0	100.00	100.00	0.00
200	2601	2601	3	0	100.00	99.88	0.12
201	1963	1962	0	1	99.95	100.00	0.05
202	2136	2135	0	3	99.86	100.00	0.14
203	2980	2973	12	7	99.77	99.60	0.64
205	2656	2656	0	0	100.00	100.00	0.00
207	1860	1860	0	0	100.00	100.00	0.00
208	2955	2948	3	7	99.76	99.90	0.34
209	3005	3005	0	0	100.00	100.00	0.00
210	2650	2649	2	1	99.96	99.92	0.11
212	2748	2748	3	4	99.85	99.89	0.25
213	3251	3251	0	0	100.00	100.00	0.00
214	2262	2262	0	0	100.00	100.00	0.00
215	3363	3362	0	1	99.97	100.00	0.03
217	2208	2207	1	1	99.95	99.95	0.09
219	2154	2154	1	1	99.95	99.95	0.09
220	2048	2048	0	0	100.00	100.00	0.00
221	2427	2427	0	0	100.00	100.00	0.00
222	2483	2483	0	0	100.00	100.00	0.00
223	2605	2605	1	0	100.00	99.96	0.04
228	2053	2051	4	5	99.76	99.81	0.44
230	2256	2256	0	0	100.00	100.00	0.00
231	1571	1571	0	0	100.00	100.00	0.00
232	1780	1780	10	0	100.00	99.44	0.56
233	3079	3077	0	2	99.94	100.00	0.06
234	2753	2753	0	0	100.00	100.00	0.00
Overall	109494 (Total)	109428 (Total)	77 (Total)	84 (Total)	99.92 (Average)	99.93 (Average)	0.15 (Average)

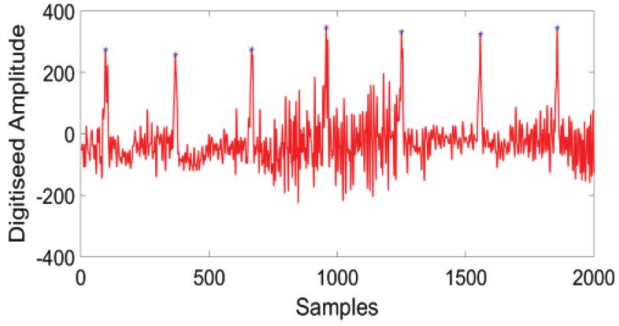

Figure 5: R-peak detection in a segment from record 104 containing severe muscular noise

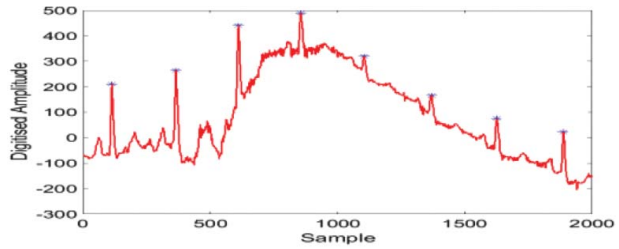

Figure 6: R-peak detection in a segment from record 121 containing large baseline wander

algorithm on ECG signals with different wave morphologies taken from records 208, 222, and 109 of the MIT BIH database, respectively. Record 208 contains

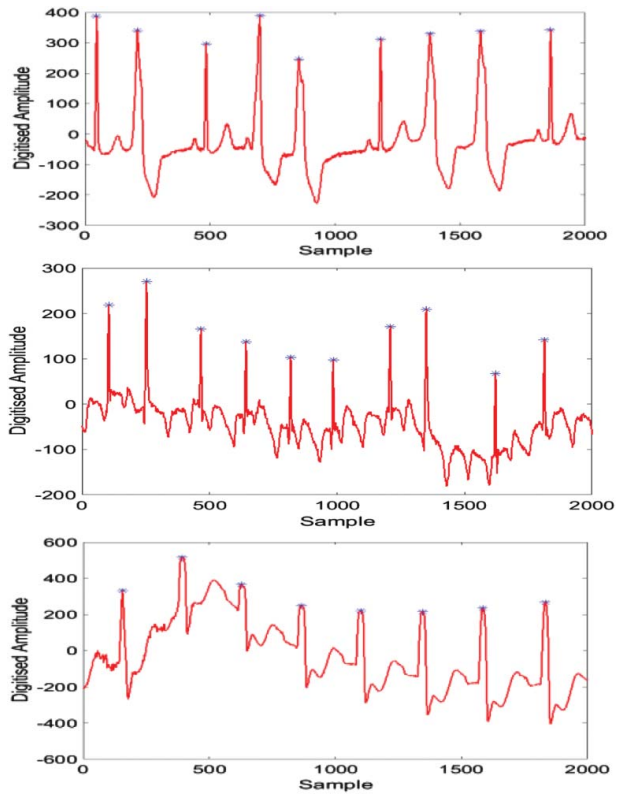

Figure 7: R-peak detection in ECG signals with different wave morphologies from records 208 (top), 222 (middle), and 109 (bottom)

Table 2: **Comparison of performance of the proposed method with other methods on the MIT-BIH arrhythmias database**

Reference	Method	FN	FP	Se (%)	P^+ (%)	DER (%)
Pan and Tompkins (1985) [10]	First derivative followed by squaring	277	507	99.54	99.75	0.712
Zidelmal et al. (2014) [19]	S-transform and Shannon energy	171	97	99.84	99.91	0.250
Martinez et al. (2004) [15]	Discrete wavelet transform	220	153	99.80	99.86	0.340
Bouaziz et al. (2014) [17]	Discrete wavelet transform	140	232	99.87	99.79	0.340
Yochum et al. (2016) [41]	Continuous wavelet transform	160	574	99.85	99.48	0.670
Phukpattaranont (2015) [18]	Quadratic filtering	202	210	99.82	99.81	0.380
Proposed method	SSWT and nonlinear transformation	84	77	99.92	99.93	0.15

premature ventricular contraction beats which have wider than normal QRS complexes with abnormal morphology. Record 222 consists of unusual wave morphologies and record 109 corresponds to left bundle branch block. The proposed algorithm detects R-peaks in all these beat types successfully. The performance of the proposed method is also compared with some established and state-of-the-art QRS detection algorithms proposed in the literature in Table 2. It can be seen that the proposed method significantly outperforms the referenced methods. It can be seen that the proposed method gives better results than the discrete wavelet transform, CWT and S-transform-based methods. However, the improved performance of the proposed method cannot be attributed to the use of the SSWT alone. The nonlinear transformation stage and the improved decision logic that uses three criteria, viz. threshold, minimum peak separation and minimum peak prominence also play a very important role.

5. CONCLUSION

In this paper, a novel technique for QRS detection in ECG signals is proposed. The detection algorithm uses the recently proposed SSWT to obtain a TFR of the ECG signal. The coefficients in the frequency range corresponding to the QRS complex are selected and reconstructed to form a signal on which further processing including a nonlinear mapping is applied to reduce false positives and negatives. The peaks are detected in the envelope of the signal thus obtained and mapped to corresponding peaks in the denoised signal. The algorithm is shown to successfully detect QRS complexes in various noise conditions and in cases of varying QRS morphologies. The algorithm is evaluated on the MIT-BIH

arrhythmia database and overall sensitivity, positive predictivity and percentage error values of 99.92%, 99.93%, and 0.15%, respectively, are obtained.

ACKNOWLEDGEMENTS

The authors would like to thank the anonymous referees whose valuable suggestions have helped in improving the quality of this paper.

DISCLOSURE STATEMENT

No potential conflict of interest was reported by the authors.

REFERENCES

1. R. M. Rangayyan, *Biomedical Signal Analysis: A Case-Study Approach*. New York: Wiley Interscience; Piscataway, NJ: IEEE Press, 2002, pp. 14.
2. S. Pal and M. Mitra, "Detection of ECG characteristic points using multiresolution wavelet analysis based selective coefficient method," *Measurment*, Vol. 43, pp. 255–61, Feb. 2010.
3. S. Banerjee, R. Gupta, and M. Mitra, "Delineation of ECG characteristic features using multiresolution wavelet analysis method," *Measurement*, Vol. 45, pp. 474–87, Apr. 2012.
4. S. Bannerjee and M. Mitra, "Application of cross wavelet transform for ECG pattern analysis and classification," *IEEE Trans. Instrum. Meas.*, Vol. 63, pp. 326–33, Feb. 2014.
5 S. -N. Yu and Y. -H. Chen, "Noise-tolerant electrocardiogram beat classification based on higher order statistics of subband components," *Artif. Intell. Med.*, Vol. 46, pp. 165–78, Jun. 2009.
6. C. Ye, B. V. K. V. Kumar, and M. T. Coimbra, "Heartbeat classification using morphological and dynamic features of ECG signals," *IEEE Trans. Biomed. Eng.*, Vol. 59, pp. 2930–41, Oct. 2012.
7. M. Daud, P. Ravier, R. Harba, M. Jabloun, B. Yagoubi, and O. Buttelli, "HRV spectral estimation based on constrained Gaussian modeling in the nonstationary case," *Biomed. Signal Process. Control*, Vol. 8, pp. 483–90, Nov. 2013.
8. E. Gil, M. Mendez, J. M. Vergara, S. Cerutti, A. M. Bianchi, and P. Laguna, "Discrimination of sleep-apnea- related decreases in the amplitude fluctuations of PPG signal in children by HRV analysis," *IEEE Trans. Biomed. Eng.*, Vol. 56, pp. 1005–14, Apr. 2009.
9. B. U. Kohler, C. Hennig, and R. Orglmeister, "The principles of software QRS detection," *IEEE Eng. Med. Biol. Mag.*, Vol. 21, pp. 42–57, Jan.–Feb. 2002.
10. J. Pan and W. J. Tompkins, "A real-time QRS detection algorithm," *IEEE Trans. Biomed. Eng.*, Vol. 32, pp. 230–5, Mar. 1985.
11. Y. H. Hu, W. J. Tompkins, J. L. Urrusti, and V. X. Afonso, "Applications of artificial neural networks for ECG signal detection and classification", *J. Electrocardiol.*, Vol. 26, pp. 66–73, 1993.
12. G. Vijaya, V. Kumar, and H. K. Verma, "ANN-based QRS-complex analysis of ECG," *J. Med. Eng. Technol.*, Vol. 22, pp. 160–7, Jul.–Aug. 1998.
13. K. Arbateni and A. Bennia, "Sigmoidal radial basis function ANN for QRS complex detection," *Neurocomputing*, Vol. 145, pp. 438–50, Dec. 2014.
14. C. Li, C. Zheng, and C. Tai, "Detection of ECG characteristic points using wavelet transforms," *IEEE Trans. Biomed. Eng.*, Vol. 42, pp. 21–8, Jan. 1995.
15. J. P. Martinez, R. Almeida, S. Olmos, A. P. Rocha, and P. Laguna, "A wavelet-based ECG delineator: Evaluation on standard databases," *IEEE Trans. Biomed. Eng.*, Vol. 51, pp. 570–81, Apr. 2004.
16. Z. Zidelmal, A. Amirou, M. Adnane, and A. Belouchrani, "QRS detection based on wavelet coefficients," *Comput. Methods Programs Biomed.*, Vol. 107, pp. 490–6, Sep. 2012.
17. F. Bouaziz, D. Boutana, and M. Benidir, "Multiresolution wavelet-based QRS complex detection algorithm suited to several abnormal morphologies," *IET Signal Process.*, Vol. 8, pp. 774–82, Sep. 2014.
18. P. Phukpattaranont, "QRS detection algorithm based on the quadratic filter," *Expert Syst. Appl.*, Vol. 42, pp. 4867–77, Jul. 2015.
19. Z. Zidelmal, A. Amirou, A. Moukadem, and A. Dieterlen, "QRS detection using S-transform and Shannon energy," *Comput. Methods Programs Biomed.*, Vol. 116, pp. 1–9, Aug. 2014.
20. X. Ning and I. W. Selesnick, "ECG enhancement and QRS detection based on sparse derivatives," *Biomed. Signal Process Control*, Vol. 8, pp. 713–23, Nov. 2013.
21. M. S. Manikandan and K. P. Soman, "A novel method for detecting R-peaks in electrocardiogram (ECG) signal," *Biomed. Signal Process. Control*, Vol. 7, pp. 118–28, Mar. 2012.
22. H. Zhu and J. Dong, "An R-peak detection method based on peaks of Shannon energy envelope," *Biomed. Signal Process Control*, Vol. 8, pp. 466–74, Sep. 2013.
23. G. Thakur, E. Brevdo, N. S. Fuckar, and H. -T. Wu, "The synchrosqueezing algorithm for time-varying spectral analysis: Robustness properties and new paleoclimate applications," *Signal Process.*, Vol. 93, pp. 1079–94, May 2013.
24. R. H. Herrera, J. B. Tary, M. Van Der Baan, et al., "Body wave separation in the time-frequency domain," *IEEE Trans. Biomed. Eng.*, Vol. 12, pp. 364–68, Feb. 2015.
25. P. Wang, J. Gao, and Z. Wang, "Time-frequency analysis of seismic data using synchrosqueezing transform," *IEEE Geosci. Remote Sens. Lett.*, Vol. 11, no. 12, pp. 2042–4, Dec. 2014.
26. M. Mihalec, J. Slavič, and M. Boltežar, "Synchrosqueezed wavelet transform for damping identification," *Mech. Syst. Signal Process.*, Vol. 80, pp. 324–34, Dec. 2016.
27. H.T. Wu, Y.H. Chan, Y.T. Lin, and Y.H. Yeh, "Using synchrosqueezing transform to discover breathing dynamics from ECG signals," *Appl. Comput. Harmon. Anal.*, Vol. 36, pp. 354–9, Mar. 2014.
28. M. M. Kabir and L. G. Tereshchenko, "Development of analytical approach for an automated analysis of continuous long-term single lead ECG for diagnosis of paroxysmal atrioventricular block," in *Proceedings of the Computing in Cardiology Conference*, Cambridge, MA, Sep. 2014, pp. 913–6.

29. I. Daubechies and S. Maes, "A nonlinear squeezing of the continuous wavelet transform based on auditory nerve models," in *Wavelets in Medicine and Biology*, A. Aldroubi and M. Unser, Eds. Boca Raton, FL: CRC Press, 1996, pp. 527–46.
30. F. Auger and P. Flandrin, "Improving the readability of time-frequency and time-scale representations by the reassignment method," *IEEE Trans. Signal Process.*, Vol. 43, pp. 1068–89, May 1995.
31. E. C- Mottin, F. Auger, and P. Flandrin, "Time-frequency/time-scale reassignment," in *Wavelets and Signal Processing*, L. Debnath Ed. in: *Appl. Numer. Harmon. Anal.*, Boston, MA: Springer, 2003, pp. 233–67.
32. E. C- Mottin, I. Daubechies, F. Auger, and P. Flandrin, "Differential reassignment," *IEEE Signal Process. Lett.*, Vol. 4, pp. 293–4, Oct. 1997.
33. I. Daubechies, J. Lu, and H. T. Wu, "Synchrosqueezed wavelet transforms: An empirical mode decomposition-like tool," *Appl. Comput. Harmon. Anal.*, Vol. 30, pp. 243–61, Mar. 2011.
34. N. E. Huang, Z. Shen, S. R. Long, M. C. Wu, H. H. Shih, Q. Zheng, N. C. Yen, C. C. Tung, and H. H. Liu, "The empirical mode decomposition and the Hilbert spectrum for nonlinear and non-stationary time series analysis," *Math. Phys. Eng. Sci.*, Vol 454, no. 197, pp. 903–95, Mar. 1998.
35. J. Xiao and P. Flandrin. "Multitaper time-frequency reassignment for non-stationary spectrum estimation and chirp enhancement," *IEEE Trans. Signal Process.*, Vol. 55, pp. 2851–60, Jun. 2007.
36. H. Yang., "Robustness analysis of synchrosqueezed transforms," *arXiv:1410.5939 [math.ST]*, Oct. 2014.
37. I. Dmytro, P. VE McClintock, and A. Stefanovska, "Linear and synchrosqueezed time–frequency representations revisited: Overview, standards of use, resolution, reconstruction, concentration, and algorithms," *Digital Signal Process.*, Vol. 42, pp. 1–26, Jul. 2015.
38. H. Yang, "Synchrosqueezed wave packet transforms and diffeomorphism based spectral analysis for 1D general mode decompositions," *Appl. Comput. Harmon. Anal.*, Vol. 39, pp. 33–66, Jul. 2015.
39. MIT-BIH Arrhythmias Database, Available: http://www.physionet.org/physiobank/database/mitdb
40. MATLAB Synchrosqueezing Toolbox, Available: https://web.math.princeton.edu/∼ebrevdo/synsq/ (posted June, 2012)
41. M. Yochum, C. Renaud, and S. Jacquir, "Automatic detection of P, QRS and T patterns in 12 leads ECG signal based on CWT," *Biomed. Signal Process Control.*, Vol. 25, pp. 46–52, Mar. 2016.

Authors

Tanushree Sharma received her BE (honors) degree in electronics and communication engineering from Rajasthan University in the year 2005. She received her MTech (honors) degree from Rajasthan Technical University in digital communication systems in the year 2011. She is currently pursuing her PhD degree in signal processing at Malaviya National Institute of Technology, Jaipur, in the Department of Electronics and Communication Engineering. She has over eight years of teaching experience in the capacity of lecturer and an assistant professor. Her research interests include signal processing and machine learning.

E-mail: tanushreesharma1@gmail.com

Kamalesh Kumar Sharma received BE and ME (honors) degrees in electronics and communication engineering from Malaviya National Institute of Technology, Jaipur, India, in 1990 and 2001, respectively. He completed his PhD degree from Indian Institute of Technology, Delhi in the year 2008. Presently, he is working as a professor and Head with the Department of Electronics and Communication Engineering, Malaviya National Institute of Technology. His research interests include sampling theory of signals, signal and image processing and fractional transforms. Mr Sharma is a life member of I.E.T.E., India.

E-mail: kksharma_mrec@yahoo.com